12 Annual Conference of the Materials Research Society of Serbia, Herceg Novi, Montenegro, September 6–10, 2010

Samarium-Doped Ceria Nanostructured Thin Films Grown on FTO Glass by Electrodepostion

Lj.S. Živković[a,b,*], V.Lair[a], O. Lupan[a,c], M. Cassir[a], A. Ringuedé[a]

[a]Laboratorie d' Electrochimie, Chimie des Interfaces et Modélisation pour l'Énergie, LECIME, CNRS UMR 7575-ENSCP-Paris, 11 rue Pierre et Marie Curie, 75231 Paris cedex 05, France

[b]The Vinča Institute of Nuclear Sciences, University of Belgrade, PO BOX 522, 11 001Belgrade, Serbia

[c]Department of Microelectronics and Semiconductor Devices, Technical University of Moldova, 168 Stefan cel Mare Blvd., Chisinau, MD-2004, Republic of Moldova

Electrical, optical or catalytic properties of ceria can be tuned via doping by rare earth elements. The innate properties of ceria-based materials can be further amplified by using nanostructured ceria. In this study, Sm-doped ceria (SDC) coatings were grown on the FTO glass substrate by means of cathodic deposition. Films were obtained from mixed Sm^{3+}/Ce^{3+} aqueous nitrate solutions, applying -0.8V/(SCE) potential for 1 h. Selected conditions gave rise to adherent, homogeneous and well-covering nanostructured SDC thin films. EDX analysis showed that 0.8 and 1.5 mol% Sm^{3+} led to 3.4 and 6.3 at.% Sm in the SDC films. XRD and Raman analysis confirmed the formation of cubic fluorite-type CeO_2. However, Sm-doping decreased the crystallite size of nanostructured ceria. The effect of annealing on SDC film was also studied. An improvement in crystallite quality was found with increasing temperature. Optical absorption properties were studied and the band gap value (E_g) of 3.07 eV was determined for pure ceria. Sm-doped ceria exhibited a red shifting. The E_g values were 2.97 and 2.81 eV, in due order.

PACS: 81.15.Pq, 68.55.Ln, 61.46Km, 78.67.–n

1.Introduction

Ceria and ceria-based materials have been attracting academic and technological attention owing to a wide range of their applications in heterogeneous catalysis, oxygen gas sensors, solid electrolyte fuel cells, and especially, three way catalysts for automobile exhaust systems [1–5]. High performance of ceria is largely based on the ease of reducing Ce^{4+} to Ce^{3+}, high oxygen storage capacity, and high oxygen ion conductivity. Ceria also displays optical properties, which are of great interest for its application. Having band gap energy of ca. 3eV, it exhibits a unique absorbing ability in the ultraviolet range and is used as a blocking material in the UV-shielding [6, 7]. Physical and chemical properties of ceria can be tuned by doping. Great attention has been focused on the doping of ceria by rare earth elements, found to bring an improvement in its electrical, optical, magnetic or catalytic properties [8–10]. In addition, during the past decades, it has been demonstrated that the intrinsic properties of these materials can be further amplified by their nanostructures of specially designed morphologies, in particular a (1D) [11,12]. Naturally, there is an ongoing interest in production of ceria-based low dimensional nanostructures as well, because of their great potentialities as catalysts, sensors, or building blocks in novel devices [13–15]. However, building a pathway to combine both of these advantages, morphology and dopant effect, represents nowadays a research challenge.

Chemical methods are recognized as a promising route to the fabrication of a variety of ceria nanostructures, although often requiring long or harsh experimental conditions [16–19]. Our group has demonstrated recently that a rod-like nanostructured-ceria film can be grown on FTO glass substrate by electrochemical deposition process (ECD) [20]. ECD is a cost-effective technique suitable for producing high-quality ceria thin films. It provides an easy way to monitor process parameters and tailor coating characteristics. The method is based on the reduction of oxygen precursor to form hydroxide ions in the vicinity of the working electrode. In the case of ceria synthesis, the OH^- ions react with the Ce^{3+} cations present in the electrolytic solution, forming, via either $Ce(OH)_2^{2+}$ dehydration or $Ce(OH)_3$ oxidation, a thin oxide layer on the surface of the working electrode [21, 22]. Cathodic method is also applicable to other metal cations taking part in the precipitation at high pH, such as Sm^{3+}. Many teams detailed the ECD of ceria, but only a few studies deal with SDC and Sm films [23–26].

The current study, as an extension of our previous work [20], reports on the possibility of doping nanostructured ceria by Sm^{3+}, in view of enhancing its UV-

* corresponding author; e-mail: ljzivkovic@vinca.rs

shielding or catalytic properties. Two Sm^{3+} concentrations were added into the electrochemical bath and their final quantity in grown films was determined. We focus on the effect of the Sm doping on the structural and optical properties of deposited films. The crystal structure evolution, as a function of annealing temperature, is detailed for SDC film. This is an important feature, as for viable applications thermally and chemically stable CeO_2 layers are desirable.

2. Experimental

The electrolyte was composed of 5 mM $Ce(NO_3)_3 \cdot 6H_2O$ (Alfa Aesar, 99.5%), with or without addition of 0.8 and 1.5% $Sm(NO_3)_3 \cdot 6H_2O$ (Alfa Aesar,99.99%) (calculated on the Ce^{3+} molar basis), with 0.1 M KNO_3 (Riedel de Haen) as a supporting electrolyte. It was saturated with molecular oxygen prior to the electrolysis and the O_2 bubbling was kept on during the growth process. The temperature was fixed at 30 °C. ECD of ceria-based layers was achieved in a three-electrode cell. The counter electrode was a platinum wire and the reference was a saturated calomel electrode (SCE). Coatings were grown on the F:SnO_2 (FTO) coated glass substrate, used as a working electrode. The substrate was prepared as detailed in Ref. 20. To ensure a deposition as homogeneous as possible, the substrate was fixed to a rotating electrode (300 rotations per minute). ECD was carried out potentiostatically, at -0.8 V/SCE for 1 h. An EG&G PAR unit, model 263A was used. As-grown films were washed with water. Thermal annealing was done in a tubular furnace, heating rate 2 °C/min. XRD was performed by a Siemens D5000 instrument (with 40 kV and 45 mA generator settings in the 2θ range between 10 and 100°). The average crystallite size was determined using X'pert Database 32 software. SEM images were taken using a high resolution Ultra 55 Zeiss FEG scanning electron microscope. Energy dispersive X-ray spectroscopy (EDX) analysis was performed with a Bruker Li-drift silicon detector. The quantification of Sm and Ce was done using standards (SmF_3 and $CeAl_2$). Micro-Raman spectra were registered by a Horiba Jobin system (HR800UV). Optical absorbance measurements were performed in the wavelength range from 300 to 1100 nm using a Cary 50 (Varian) UV-Vis-NIR spectrophotometer.

3. Results and discussion

3.1. Electrochemical deposition and composition analysis of deposited films

Figure 1 shows the variation of current density, j, with time, during the electrodeposition process of ceria-based films, with or without Sm-addition. The overall shape of the curves is similar. An important feature is a well-defined cathodic wave, to be assigned to the nucleation-growth process. The presence of this wave at rather short deposition time is typically observed for films of good crystallographic quality and coverage [27]. With increasing Sm concentration, the wave becomes less and less pronounced and moves towards lower values of current densities. The reduction in peak maximum can be attributed to the diminution of ceria nucleation sites density in the presence of samarium. This electrochemical behavior can be explained by the formation of low-conductivity Sm-based layers on the electrode surface, which retards the oxygen reduction process, in analogy with literature [26, 28, 29].

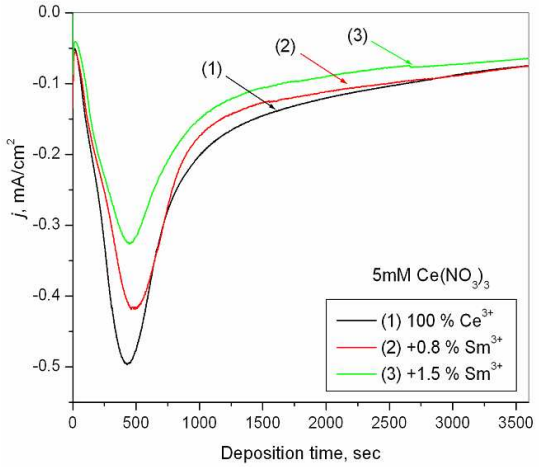

Fig. 1. Current-transients for Ce-based film growth as a function of Sm^{3+} concentration in Ce^{3+} bath.

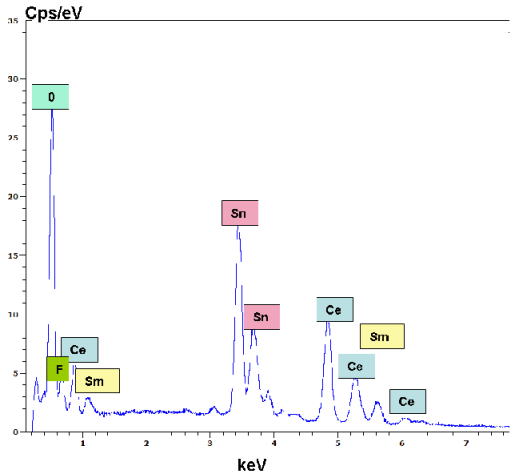

Fig. 2. EDX spectrum of SDC2 film grown from 1.5% Sm^{3+} added into Ce^{3+} bath.

Figure 2 illustrates a typical EDX spectrum for the SDC film deposited on FTO glass. The Ce signals were registered at 0.9, 4.9, 5.3 and 6.0 keV and Sm peaks at 1.1 and 5.6 keV, giving the final composition (at.%) of 96.6% Ce + 3.4% Sm and 93.7% Ce + 6.3% Sm in the SDC films grown from 0.8 and 1.5 mol% Sm in deposition bath, respectively. The films are referred to as SDC1 and

SDC2 in the further text. Peaks corresponding to Sn and F, originating from FTO substrate, are also observed in the EDX spectrum.

3.2. Morphology and structural characterization of the films

As an example of SDC film microstructure, a SEM micrograph of SDC2 is given in Fig. 3. The coating is well covering and adherent, Fig. 3(a). It is around 250 nm in thickness. Although some cracks appear in all samples, they are more pronounced in pure than in Sm-doped ceria films. All ceria-based coatings are nanostructured materials. The rod-like grain shape is a dominant feature, Fig. 3(b). Rod-like grains are up to 700 nm in length and ca. 100 nm in radius. However, this rod-like shape is not so well defined as that grown from 2x lower electrolyte concentration [20]. According to XRD findings, grains are not single crystals, but consist of smaller subunits. In addition, plate-like grains coexist in SDC films. Grains of bigger size could originate from the decreased number of ceria nucleation centres, due to the presence of Sm. This hypothesis requires further experimental proofs. Indeed, shape evolution of ceria nanocrystals is very complex and still not fully defined, as governed by multiple parameters: reaction time, reaction temperature, reactant concentrations etc. [19, 31].

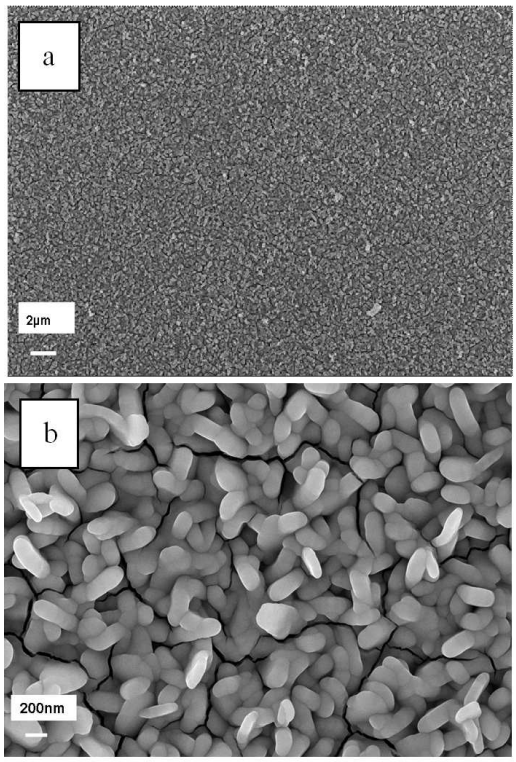

Fig. 3. SEM view of SDC2 microstructure.

Figure 4 illustrates XRD patterns for as-grown ceria and SDC films. Diffraction peaks corresponding to (111), (200), (220) and (311) crystallographic planes were registered for all samples and are identified as face-centred cubic CeO_2 phase, referring to the standard data JCPDS 34 0394. When CeO_2 was doped with Sm, all diffraction peaks can still be indexed to the cubic structure, curves (2) and (3). However, broadening of the peaks and a decrease in their intensity are observed with increasing Sm doping. These observations can be associated with a decrease in crystallinity or a diminution in the crystallite size. The average crystallite size was determined for all samples and was found to decrease accordingly. Size values of 20.2, 18.2 and 15.8 nm were determined for ceria, SDC1 and SDC2 crystallites, respectively. Figure 5 shows in parallel the diffraction peaks for as grown and annealed (1h at 600 °C) SDC1 sample. It is clearly seen that the reflection peaks become sharper and narrower with annealing, indicating better defined film crystallinity after the thermal treatment. Analogous finding for as-grown and annealed films has been confirmed for all samples.

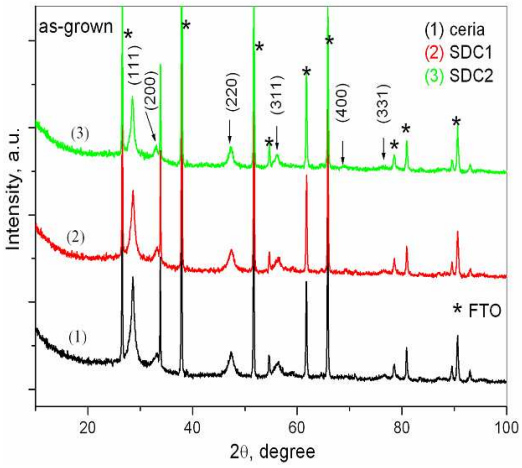

Fig. 4. XRD patterns of as-grown ceria-based films as a function of Sm amount.

Raman spectroscopy completed the structural characterization of ceria-based coatings. Figure 6 shows the spectra of pure and Sm-doped coatings after annealing at 600 °C, 1 h. The most intense band for pure ceria (curve (1)) appears at about 465 cm^{-1} and corresponds to the F2g Raman active-mode of fluorite structure [31]. In the case of CeO_2 doped with Sm, the maximum of major peak moves very slightly towards lower frequencies, from 465 to 463 cm^{-1}. This shift is ascribed to the lattice constriction and the change in crystal environment caused by SDC solid solution formation [9, 10]. Moreover, with increasing amount of Sm, the Raman peak becomes broader and an increase in full width at half maximum (FWHM) is observed. This result is in close agreement with XRD data presented above. The evolution of the crystal structure with annealing temperature was studied for SDC2 film, and is illustrated in Fig. 7. For the as-grown film, the major Raman band is

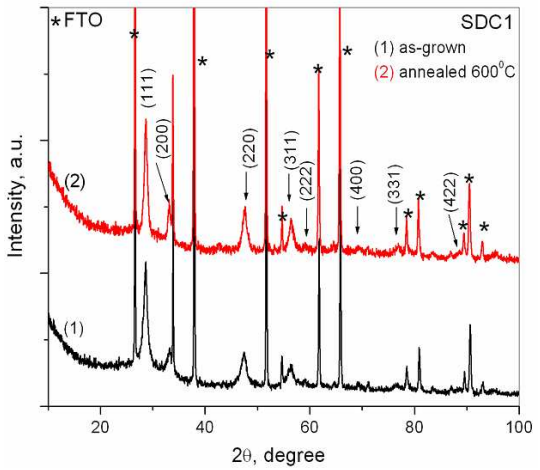

Fig. 5. XRD patterns of as-grown and annealed SDC1 film.

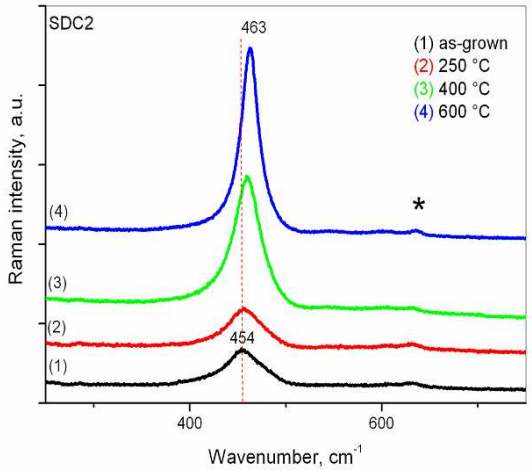

Fig. 7. Effect of annealing temperature on Raman spectra for SDC2 film.

positioned at 454 cm^{-1}. With temperature increase, the peak moves towards higher frequencies, with an overall shift of ca. 10 cm^{-1}. The peak symmetry becomes better defined and its width gradually decreases while the intensity increases. This indicates that thermal annealing induces good quality in crystal structure of the SDC material. A shoulder at around 600 cm^{-1} is also visible in the spectra. This band, principally observed in doped ceria, is attributed to the oxygen vacancies created by incorporation of the dopant. This finding represents a further evidence of SDC formation.

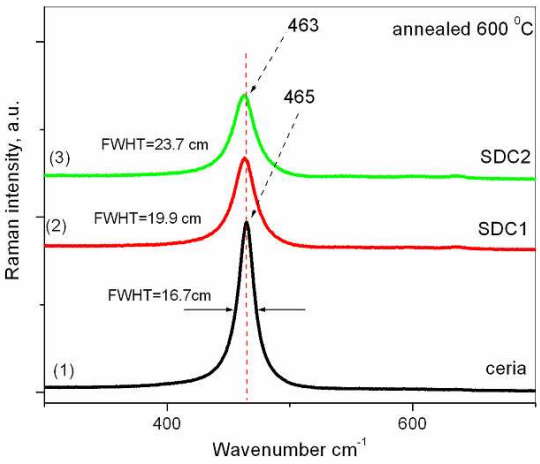

Fig. 6. Change in Raman spectra for ceria-based film with Sm-doping.

3.3. Optical characterization of the films

Figure 8 shows UV vis absorption spectra recorded for ceria-based films, grown on the FTO substrate, as a function of Sm doping. As can be seen, there is a strong absorption band below 400 nm in the spectrum for pure ceria film (curve (1)), originating from the charge-transfer transition between $O^{2-}(2p)$ and $Ce^{4+}(4f)$ orbitals in CeO_2 [31]. However, with Sm^{3+} doping, the absorption band exhibits red shifting compared with ceria film, curves (2) and (3), for SDC1 and SDC2 samples, respectively. Red shifting for doped ceria nanocrystals results from a decrease in the valence charge from Ce^{4+} to Ce^{3+}, caused by replacement of the Ce^{3+} fraction on the CeO_2 surface by trivalent Sm^{3+} ions [9, 10].

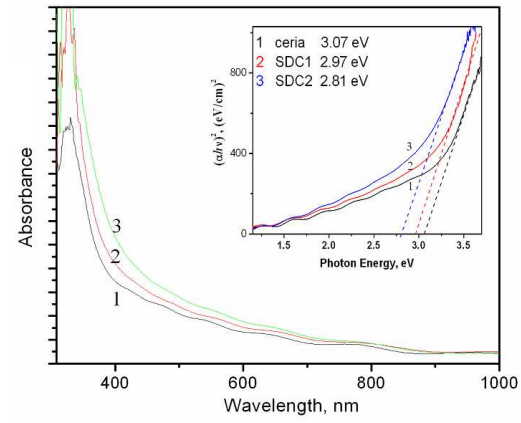

Fig. 8. UV-vis spectra of ceria-based films: (1) pure ceria, (2) SDC1 and (3) SDC2. Inset illustrates plots of $(\alpha h\nu)^2$ *vs.* photon energy.

Indirect optical band gap energy (E_g) for ceria particles was determined by fitting the absorption data to the direct transition equation [32, 33]:

$$\alpha h\nu = A(h\nu - E_g)^{1/2} \quad (1)$$

where α is the absorption coefficient ($4\pi k/\lambda$), and A is the constant.

The optical band gap value was obtained by extrapolating the linear part of the curve $(\alpha h\nu)^2$ as a function of incident photon energy, $h\nu$, to intercept the energy x-

axis at $\alpha = 0$. The plots $(\alpha h\nu)^2$ vs. photon energy $(h\nu)$ are given as an inset in Fig. 9. The following E_g values of 3.07, 2.97 and 2.81 eV were determined for pure and Sm-doped (3.4 and 6.3 at.% Sm) ceria nanostructures, respectively. Our result is consistent with reported E_g values [10].

Conclusion

This work demonstrates that nanostructured SDC films can be directly formed from nitrate solutions at room temperature by electrodeposition method. Thin SDC films were grown on conductive FTO glass in potentiostatic mode, applying a potential of −0.8 V/SCE for 1h. Raman and XRD analysis confirmed the formation of a well-crystalline Sm-ceria solid solution, exhibiting a cubic fluorite-type CeO_2 structure. Addition of 0.8 and 1.5 mol% Sm^{3+} into the electrochemical solution led to the incorporation of 3.4 and 6.3 at.% Sm into SDC, as confirmed by EDX analysis. Morphology of the film exhibits mainly rod-like grains of ca. 100 nm in radius, and up to 700 nm in length. It was found that thermal annealing contributed to better crystallinity and crystal quality of the SDC films. Optical absorption properties were also studied. The Sm-doping was shown to shift the ceria band gap, $E_g = 3.07$ eV, towards lower values of photon energy, 2.97 and 2.81 eV, respectively.

Acknowledgments

This work was supported by ANR (Agence National de la Recherche-France) ANR JCJC06-0131 COMICEL program. Dr. L. Živković acknowledges CNRS for the research position and also thanks the Ministry of Science of the Republic of Serbia (Pr. No 45012).

References

[1] T. Taniguchi, *Cryst. Growth Des.* **8**, 3725 (2008).

[2] M. Primet, E. Garbowski in: *Catalysis by Ceria and Related Materials*, Ed. A. Trovarelli, Imperial College Press, London 2002, p. 407.

[3] B.C.H. Steele, *Solid State Ionics* **129,** 95 (2000).

[4] N. Izu, N. Marayama, W. Shin, I. Matsubara, S. Kanzaki, *Jpn. J. Appl. Phys.* **43**, 6920 (2004).

[5] R. Di Monte, J. Kaspar, *J. Mater. Chem.* **15,** 633 (2005).

[6] S. Tsunekawa, T. Fukuda, *J. Appl. Phys.* **87**, 1318 (2000).

[7] M. Yamashita, K. Kameyama, S. Yabe, Y. Yoshida, Y. Fujishiro, T. Kawai, T. Sato, *J. Mater. Sci.* **37,** 683 (2002).

[8] S. Fujihara, M. Oikawa, *J. Appl. Phys.***95,** 8002 (2004).

[9] Y. Wang, Z. Quan, J. Lin, *Inorg. Chem.* **46,** 5237 (2007).

[10] G.–R. Li, D.–L. Qum, L. Arurault, Y.–X. Tong, *J. Phys. Chem. C* **113,** 1235 (2009).

[11] D.D. Ma, C.S. Lee, F.C.K. Au, S.Y. Tong, S.T. Lee, *Science* **299**, 1874 (2003).

[12] S.V.N.T. Kuchibhatla, A.S. Karakoti, D. Bera, S. Seal, *Progress Mater. Sci.* **52**, 699 (2007).

[13] K. Zhou, X. Wang, X. Sun, Q.J. Peng, Y. Li, *J. Catalysis* **229,** 206 (2005).

[14] Z.–Y. Yuan, V. Idakiev, A. Vantomme, T. Tabakova, T-Z. Ren, B-L. Su, *Catalysis Today* **131**, 303 (2008).

[15] X.–S. Huang, H. Sun, L.–Cun, Wang, Y.–M. Liu, K.–N. Fan, Y. Cao, *Appl. Catal. B: Environ.* **90,** 224 (2009).

[16] C. Sun, H. Li, Z.H. Wang, L. Chen, X. Huang, *Chem. Lett.* **33**, 662 (2004).

[17] C. Pan, D. Zhang, L. Shi, *J. Solid State Chem.* **281**, 1298 (2008).

[18] H.X. Mai, L.–D. Sun, W. Zhang, R. Sui, Y.W. Feng, H.–P. Zhang, *J. Phys.Chem. B* **109**, 24380 (2005).

[19] Q. Yuan, H.–Hong Duan, L.–L. Li, L.–D. Sun, Y.–W. Zhang, C.–H. Yan, *J. Coll. Inter. Sci.* **335,** 151 (2009).

[20] L. Čerović, V. Lair, O. Lupan, M. Cassir, A. Ringuedé, *Chem.Phys. Lett.* **494,** 237 (2010).

[21] I. Zhitommirsky, A. Petric, *Ceram. Inter.* **27**, 149 (2001).

[22] J. Schwitzer, *J. Am. Ceram. Bull.* **666**, 1521 (1987).

[23] S. Phok, R. Bhattacharya, P. Spagnol, T. Chaudhuri, *J. Electrochem. Soc.* **153**, C2736 (2006).

[24] S. Phok, R. Bhattacharya, *Phys. Status Solidi A* **203**, 3734 (2006).

[25] K. Kamada, N. Enomoto, J. Hojo, *Electrochim. Acta* **54**, 6996 (2009).

[26] E.J. Ruiz, R. Ortega-Borges, L. Godinez, T.W. Chapman, Y. Meas-Vong, *Electrochim. Acta* **52**, 914 (2006).

[27] T. Pauporté, D. Lincot, *Electrochim. Acta* **45**, 3345 (2000).

[28] A. Gaux, T. Pauporté, D. Lincot, *J. Electroanal. Chem.* **587**, 193 (2006).

[29] A. Gaux, T. Pauporté, D. Lincot, *Electrochim. Acta* **53**, 50 (2007).

[30] D. Zhang, H. Fu, L. Shi, C. Pan, Q. Li, Y. Chu, W. Yu, *Inorg. Chem.* **46,** 2446 (2007).

[31] J.R. McBride, K.C. Hass, B.D. Poindexter, W.H. Weber, *J. Appl. Phys.* **762**, 435 (1994).

[32] S. Tsunekawa, T. Fukuda, A. Kassuya, *J. Appl. Phys.* **87**, 1318 (2000).

[33] O. Lupan, T. Pauporté, L. Chow, B. Viana, F. Pellé, L.K. Ono, B. Roldan Cuenya, H. Heinrich,*Appl. Surf. Sci.* **256,** 1895 (2010).